Influence of the orthotropic behaviour on defects prediction in cup drawing, reverse redrawing and expansion

Influence of the orthotropic behaviour on defects prediction in cup drawing, reverse redrawing and expansion

M C Oliveira[1], D M Neto[1], J L Alves[2] and L F Menezes[1]

[1] CEMMPRE, Department of Mechanical Engineering, University of Coimbra, Polo II, Rua Luís Reis Santos, 3030-788 Coimbra, Portugal
[2] CMEMS, Department of Mechanical Engineering, University of Minho, Campus de Azurém, 4800-058 Guimarães, Portugal

E-mail: marta.oliveira@dem.uc.pt

Abstract. Finite elements analysis is commonly used in the cans tool design since it allows predicting different sheet metal defects and instabilities that significantly affect the efficient production of beverage cans. These defects include earing, due to the material orthotropic behaviour, thinning and fracture. The numerical prediction of these kind of defects is more complex when different combinations of strain paths are involved. The process conditions considered in this work involve the drawing of a cylindrical cup, the reverse redrawing and the expansion. The two materials under analysis are an AA5352 aluminium alloy and a TH330 steel. The materials orthotropic plastic behaviour is modelled with a non-quadratic yield criterion. The results show that changes in the yield surface lead to slight changes in the earing profile and in the location were strain localization occurs. Moreover, the numerical model must describe in detail the process conditions, since they may affect the formability prediction.

1. Introduction

Formability is often used to describe the capability of a material to undergo plastic deformation to a given shape without occurrence of defects. Therefore, it is strongly limited by the occurrence of plastic instabilities associated with unstable, non-uniform deformation, such as wrinkling and necking. The strains associated with localized necking have been used in practice, since the concept of Forming Limit Diagram (FLD) was introduced to characterize the formability of thin metal sheets [1,2]. Although it is know that the FLD is strongly strain-path dependent, it is still used to assess formability in deep drawing operations, given its practical simplicity and ease of use. The concept of stress-based FLD has been proposed by several authors (e.g. see [3,4]), to avoid the strain path dependency. On the other hand, fracture can occur either with or without abrupt severe strain localization, which has led to extensive efforts devoted to the development of models capable of predicting the formability limits. Nonetheless, these improved models typically rely on the knowledge of the constitutive model that best describes the material mechanical behaviour. In the context of strain localization prediction, the yield criterion adopted plays an important role, particularly when combined with an associated flow rule, since the plastic flow is modelled by the normal to the yield surface.

The process conditions considered in this work are the ones established for the “Benchmark 1 – Failure Prediction after Cup Drawing, Reverse Redrawing and Expansion”, proposed under the Numisheet 2016 international conference [5]. The aims where the prediction: (i) of the earing and (ii) of the thickness profile, after the reverse redrawing operation; and (iii) of the failure point during the

expansion operation. Two materials with distinct orthotropic behaviour were considered, namely TH330 steel and AA5352 aluminium alloy.

The following section presents a summary of the benchmark description as well as the details concerning the numerical model used to perform the numerical simulations. The section also describes the constitutive model adopted and the procedure used to perform the parameters identification. Section 3 presents and discusses the numerical results, taking into account the experimental results reported in [5]. Finally, the main conclusion are summarized in Section 4.

2. Cup drawing, reverse redrawing and expansion

The tools for the drawing and reverse redrawing operations consist in a pressure-pad (or blank-holder), a die and a punch. The drawing die inner diameter is 118.46 mm and its shoulder radius is 2.54 mm. The drawing punch diameter is 116.84 mm and its shoulder radius is 4.06 mm. The punch of the drawing operation becomes the die in the reverse redrawing stage, with a cavity diameter of 88.49 mm and a shoulder radius of 2.54 mm. The reverse drawing punch has a diameter of 87.86 mm and a shoulder radius of 4.06 mm. All tools have the same dimensions for both materials and their details are given in [5]. The drawing and reverse redrawing operations are performed considering a constant pressure-pad force, which is also equal for both materials. The value of force for the drawing operation is 21.1 kN and for the redrawing is 16.6 kN. Regarding the expansion operation, the tools consist of a cup support tool, a clamp plate and an expansion punch. Also in this case, the tools have the same dimensions for both materials.

2.1. Finite element model

Due to geometrical and material symmetries, only a quarter of the global structure is modelled. All forming tools are considered rigid and are modelled using Nagata patches [6], which allows the use of a coarse finite element mesh, as shown in Figure 1. The contact with friction conditions are described by the Coulomb's law, using a constant friction coefficient of 0.03, as recommended by the benchmark committee. Regarding the clamping conditions, in this work, the clamp was moved until a fixed distance from the cup support. The distance between the clamp and the cup support was determined in order to avoid any deformation during the expansion stage.

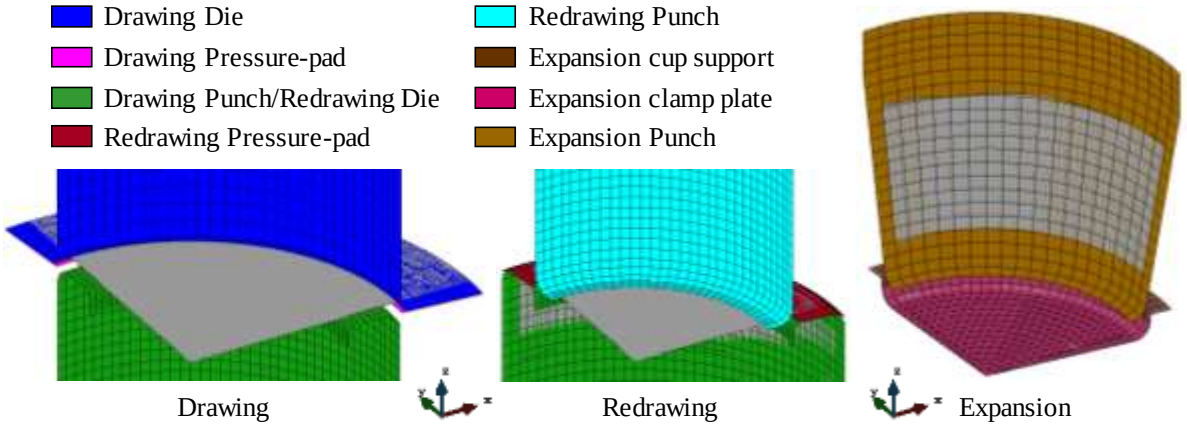

Figure 1. Numerical model: Nagata patches used to describe the surfaces of each tool.

The blank sheet is circular with a diameter of 162.97 mm. The thickness is 0.279 mm for the AA5352 and 0.270 mm for the TH330. The blank sheet is discretized with 3D 8-node hexahedral finite elements, combined with a selective reduced integration technique. The same mesh was used for both materials, which comprises a non-structured mesh for a radius lower than 36 mm (bottom of the cup) and a structured mesh for the remaining region. The mesh is composed of two layers through the thickness, which allows an accurate evaluation of the through-thickness stress gradients. The total number of elements is 11552 and the total number of nodes is 17844.

2.2. Material modelling

The mechanical behaviour of both materials is assumed to be isotropic in the elastic regime, being described by the Young's modulus, E, and the Poisson ratio, υ. Regarding the hardening behaviour, the Voce law was adopted for the AA5352 alloy, while for the TH330, the Swift hardening law was adopted. The material parameters for both hardening laws were provided by the benchmark committee, for uniaxial tensile tests performed at each 15º with the rolling direction (RD). However, it was decided to determine the best fit obtained for the uniaxial test performed at RD, imposing the yield stress valued presented for this direction. Table 1 presents the material parameters adopted and Figure 2 (a) the comparison between the hardening laws obtained for the uniaxial test performed at RD and the ones adopted in this work, for each material.

Regarding the orthotropic behaviour, the yield criterion proposed by Cazacu and Barlat in 2001 (CB2001) was adopted [7], because it is known to be flexible. The CB2001 is a generalization of the Drucker's isotropic criterion to orthotropy, which is given by:

$$\bar{\sigma} = \left\{ 27\left[\left(J_2^0 \right)^3 - c\left(J_3^0 \right)^2 \right] \right\}^{\frac{1}{6}} \tag{1}$$

where J_2^0 and J_3^0 are the second and third generalized invariants of the deviatoric Cauchy stress tensor, defined as:

$$J_2^0 = \frac{a_1}{6}(\sigma_{11}-\sigma_{22})^2 + \frac{a_2}{6}(\sigma_{11}-\sigma_{33})^2 + \frac{a_3}{6}(\sigma_{11}-\sigma_{33})^2 + a_4\sigma_{12}^2 + a_5\sigma_{13}^2 + a_6\sigma_{23}^2 \tag{2}$$

$$\begin{aligned} J_3^0 = {} & (1/27)(b_1+b_2)\sigma_{11}^3 + (1/27)(b_3+b_4)\sigma_{22}^3 + (1/27)[2(b_1+b_4)-b_2-b_3]\sigma_{33}^3 \\ & -(1/9)(b_1\sigma_{22}+b_2\sigma_{33})\sigma_{11}^2 - (1/9)(b_3\sigma_{33}+b_4\sigma_{11})\sigma_{22}^2 \\ & -(1/9)[(b_1-b_2+b_4)\sigma_{11} + (b_1-b_3+b_4)\sigma_{22}]\sigma_{33}^2 \\ & +(2/9)(b_1+b_4)\sigma_{11}\sigma_{22}\sigma_{33} - \left(\sigma_{13}^2/3\right)[2b_9\sigma_{22} - b_8\sigma_{33} - (2b_9-b_8)\sigma_{11}] \\ & -\left(\sigma_{12}^2/3\right)[2b_{10}\sigma_{33} - b_5\sigma_{22} - (2b_{10}-b_5)\sigma_{11}] - \left(\sigma_{23}^2/3\right)[(b_6-b_7)\sigma_{11} - b_6\sigma_{22} - b_7\sigma_{33}] \\ & +2b_{11}\sigma_{12}\sigma_{23}\sigma_{13} \end{aligned} \tag{3}$$

where $a_1,...,a_6$ and $b_1,...,b_{11}$ are the anisotropy parameters and c is a weighting parameter. σ_{ij}, $i,j=1,2,3$ are the stress components of the Cauchy stress tensor $\boldsymbol{\sigma}$. The conditions that guarantee the convexity of CB2001 are unknown, except when assuming in-plane isotropic behavior, for which $c \in [-3.75, 2.25]$. The a_5, a_6 and b_k $(k = 6, 7, 8, 9, 11)$ are the anisotropy parameters corresponding to the off-plane properties, that cannot be evaluated for metallic sheets. Thus, they are assumed as equal to the isotropic values, i.e. 1.0. Accordingly, it is necessary to identify a total of 10 anisotropy parameters and the c value. The anisotropy parameters were identified for both materials using the objective function and the optimization algorithm described in [8], which allows the definition of different weights for each experimental value to be fitted. Note that an associated flow rule is adopted.

In a first approach, the anisotropy parameters were identified considering a similar weighting factor for the seven *r*-values, uniaxial tension yield stresses, biaxial yield stress and r_b. The anisotropy parameters obtained are presented in Table 1 and the comparison with the experimental data is shown in Figure 2. The projection of the yield surface in the biaxial plane, assuming only non-zero stress components σ_{RD} and σ_{TD}, where RD corresponds to the rolling direction and TD to the transverse direction, is presented in Figure 2 (b). This figure highlights that for the TH330 steel, the CB2001 recovers quite well the equibiaxial yield stress (experimental value of 310 MPa and analytical value of 306.8 MPa), the r_{b} (experimental value of 0.984 and analytical of 0.983), as well as the results from the uniaxial tensile tests (see Figure 2 (c)). However, for the AA5352 alloy, the difference in the equibiaxial yield stress and r_{b} value are clear (experimental values of 242.01 MPa and 0.620; analytical values of

203.11 MPa and 0.616). This identification is labelled "AA5352" but, another was performed, increasing the weight for the equibiaxial yield stress. The parameters of the CB2001 yield criterion obtained are show in Table 1 between brackets. This identification is labelled "AA5352 (sb)" and it allows attaining analytical values for the equibiaxial yield stress and r_b value of 227.61 MPa and 0.643, respectively. Figure 2 (d) shows that both sets of anisotropy parameters lead to a similar distribution of the *r*-value, but the uniaxial yield stress values present an higher variation for the "AA5352 (sb)".

Table 1. Material parameters for the AA5352 aluminium alloy and the TH330 steel.

AA5352 aluminium alloy				TH330 steel			
Elastic properties		$Y\left(\bar{\varepsilon}^{p}\right)=Y_0+\left(Y_{sat}-Y_0\right)\left[1-\exp\left(-C_Y\bar{\varepsilon}^{p}\right)\right]$		Elastic properties		$Y\left(\bar{\varepsilon}^{p}\right)=K\left(\varepsilon_0+\bar{\varepsilon}^{p}\right)^{n}$	
E [MPa]	68500	Y_0 [MPa]	197.59	E [MPa]	205000	Y_0 [MPa]	258.87
υ	0.33	Y_{sat} [MPa]	284.09	υ	0.3	K [MPa]	577.85
		C_Y	13.46			n	0.1609
CB2001				CB2001			
a_1	1.090 (1.293)	a_2	0.860 (0.527)	a_1	1.315	a_2	0.910
a_3	1.065 (0.992)	a_4	0.980 (0.868)	a_3	0.874	a_4	1.089
b_1	2.950 (2.944)	b_2	0.323 (-0.005)	b_1	2.037	b_2	1.184
b_3	3.104 (1.704)	b_4	-1.804 (-1.882)	b_3	1.020	b_4	0.849
b_5	-1.055 (-1.170)	b_{10}	0.658 (0.244)	b_5	0.454	b_{10}	0.702
c	0.910 (1.532)			c	0.790		

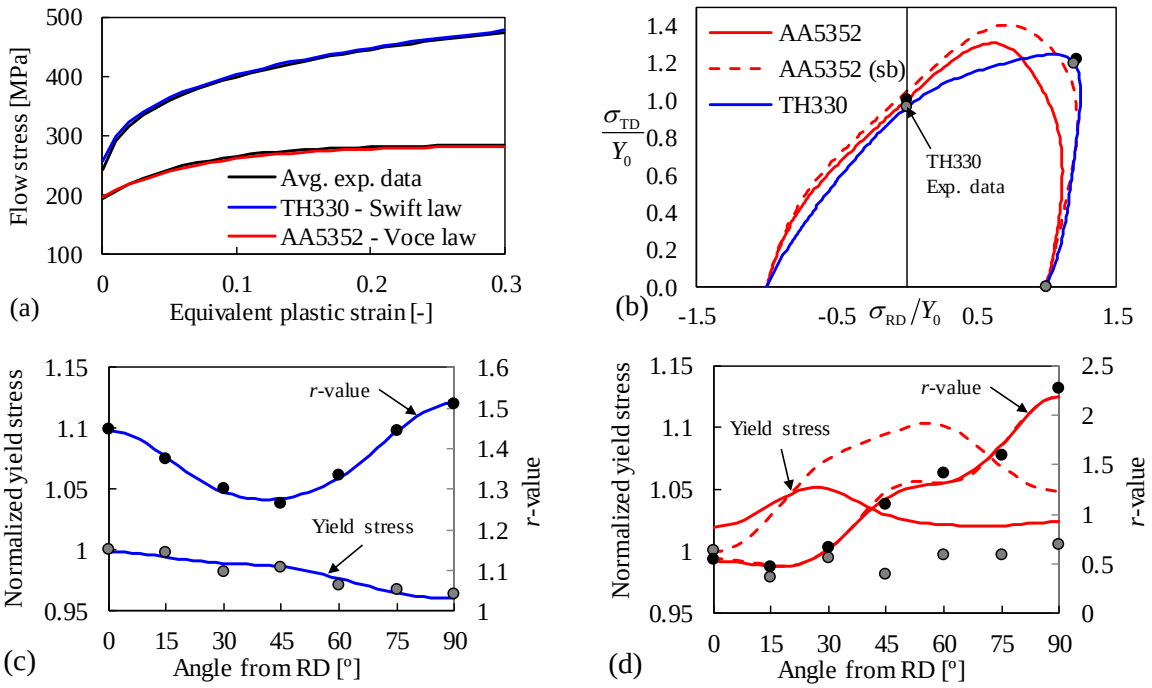

Figure 2. Numerical model: (a) comparison between the hardening laws obtained for the uniaxial test performed at RD and the ones adopted in this work; (b) projection of the yield surface in the biaxial plane; and Experimental and predicted *r*-values and yield stresses for the: (c) TH330 steel and (d) AA5352 alloy.

The description of the mechanical behaviour of the material does not include any damage model. The analysis of fracture was performed based on the occurrence of strain localization in the cup wall, during the expansion stage. The prediction of the punch displacement corresponding to the onset of failure was determined using a temporal analysis of the thickness strain and of the thickness strain rate [9]. All numerical simulations are performed with the in-house finite element solver DD3IMP [10,11]. In the following section, the numerical results are presented and discussed.

3. Results analysis and discussion

Figure 3 (a) presents the evolution of the drawing punch force with its displacement, highlighting a similar trend for both materials. The sudden decrease for approximately 25 mm of punch displacement corresponds to the instant when the sheet loses the contact with the pressure-pad. From 30 mm forward, the punch force tends to zero, when the cup is fully drawn. The "AA5352 (sb)" results in slightly higher values of force than for "AA5352", which can be related with the globally higher yield stress in-plane directionalities (see Figure 2 (c)). Figure 3 (b) presents the evolution of the reverse redrawing punch force with its stroke. Globally, the evolutions obtained present the expected trend, exhibiting a peak related with the instant the thickened area goes through the die/pressure-pad free space, which give rise to some restraining forces that must be overcome [12]. In fact, after the first stage the thickness distribution is not uniform in the cup wall, presenting values that are higher than the initial thickness in the upper part of the cup. Regarding the expansion punch force, it presents a linear trend with its stroke, as shown in Figure 3 (b). For this stage, the difference between the two sets of anisotropy parameters is negligible. Finally, it should be mentioned that the slope of the trend is clearly underestimated when compared with the experimental one, for both materials [5].

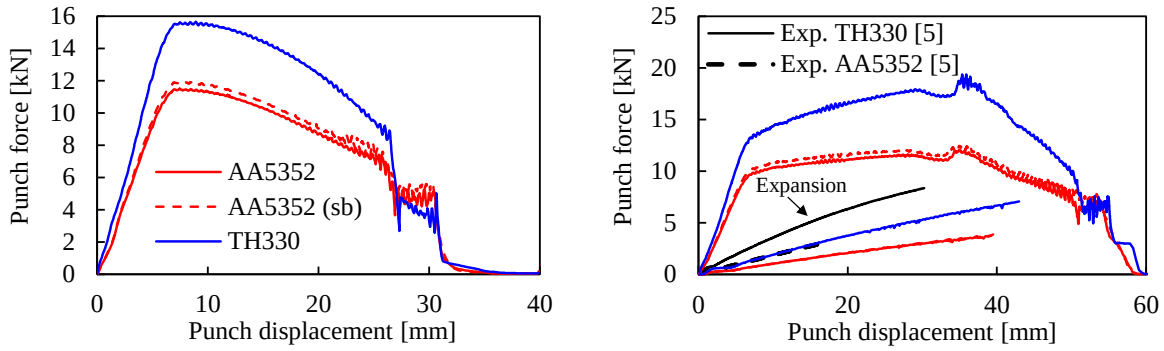

Figure 3. Punch force evolution with the displacement in the: (a) drawing and (b) reverse redrawing and expansion.

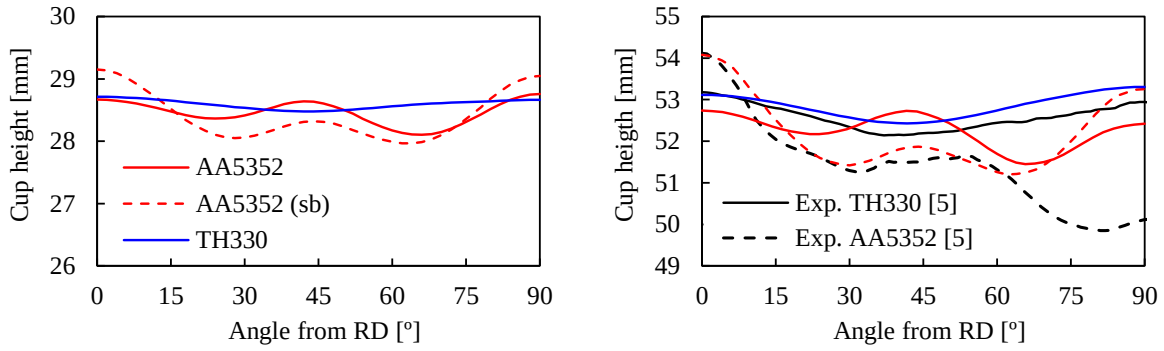

Figure 4. Cup height in function of the angle from RD at the end of the: (a) drawing and (b) reverse redrawing.

Figure 4 (a) shows the cup height at the end of the drawing stage, highlighting the almost constant value for the TH330. For the aluminium alloy, one can observe the occurrence of a total of 8 ears, which have a higher amplitude for the "AA5352 (sb)" set of anisotropy parameters. Figure 4 (b)

shows the cup height at the end of the reverse redrawing stage, confirming the presence of 4 ears for the TH330, at the same location as in the experimental results. In fact, the experimental mean height of the cup is 52.61 mm, with an amplitude of 1.14 mm (see the black continuous line in Figure 4 (b)). For the AA5352, the experimental mean height of the cup is 52.05 mm, with an amplitude of 4.13 mm (see the black dashed line in Figure 4 (b)) [5]. Although the number of ears is well predicted, the trend for the height is not well captured, because at TD it is clearly overestimated, by both sets of anisotropy parameters. As for the drawing stage, the ears present a higher amplitude for the "AA5352 (sb)", which can be related with higher amplitude for the in-plane yield stresses (see Figure 2 (d)). Nevertheless, previous results indicate that the distribution of the force imposed by the pressure-pad is quite uneven for materials presenting strong anisotropy of the *r*-values. In fact, during the drawing stage the blank-holder force is mainly concentrated closer to TD, since it is the one presenting a higher thickening, due to the effect of the lower *r*-value (see Figure 2 (d)) [8]. The same trend can also be observed in the reverse redrawing stage. With the decrease of the flange length, the gap between the die and the pressure-pad starts to decrease, in order to keep the force value constant. If this gap is not controlled it can lead to the severe thinning of the last areas of material in contact with the pressure-pad. In the numerical simulations performed, the control of the drawing pressure-pad was able to minimize this effect, but the same is not valid for the redrawing pressure-pad. Thus, as shown in Figure 5, at the end of this stage there are some areas with strong thinning at the top of the cup. For "AA5352" this occurs at the RD and close to 45º with RD, while for "AA5352 (sb)" it disappears for 45º but appears at TD, and becomes more relevant at the RD. The occurrence of this effect also contributes to the changes in the cup height. Finally, the experimental cups show that the metal at RD and 180º with RD was severely thinned [5]. Thus, although this behaviour is affected by the mechanical behaviour, this analysis highlights the importance of an accurate description of the process conditions to enable a proper comparison of numerical and experimental results.

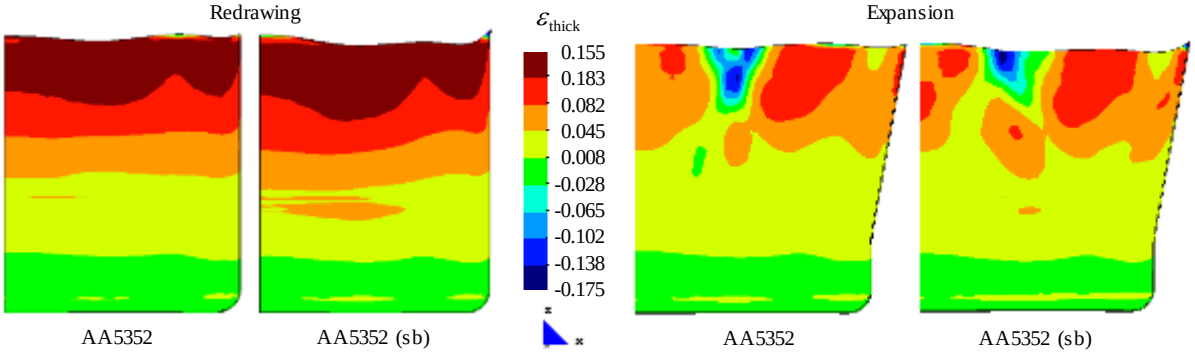

Figure 5. Distribution of the thickness strain at the end of the reverse redrawing and for the same punch displacement in the expansion phase, for the AA5352 aluminium alloy.

The thickness profile was measured after the reverse redrawing operation, at 20 mm and 45 mm from the base of the cup. Figure 6 (a) presents the results at 20 mm and (b) at 45 mm, for both materials. As expected, there is an increase of the thickness along the cup wall. Globally, the numerical simulation results underestimate the thickness evolution from the RD to the TD. In fact, for the TH330 steel the numerical values are always bellow the experimental range (see the black continuous lines in Figure 6). For the AA5352, the numerical values are close to the minimum value of the experimental range (see the black dashed lines in Figure 6). In particular, the experimental results present an increasing trend between RD and TD, while the numerical present an almost constant value. In this context, it should be mentioned that the gap between the die and the punch of the redrawing stage is equal to 0.315 mm. Thus, in the numerical simulations performed with the aluminium alloy there was some ironing of the vertical wall during the redrawing stage. This does not seems to happen in the experimental results, which indicates a slightly higher gap between the redrawing die and punch.

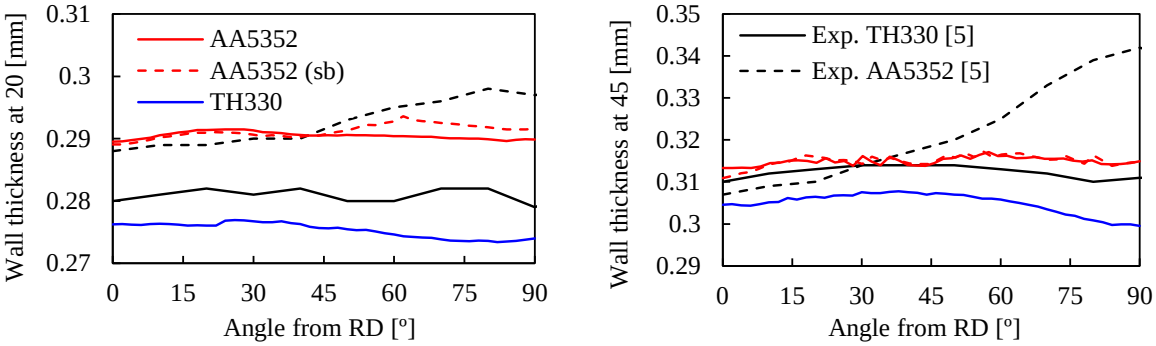

Figure 6. Wall thickness in function of the angle from RD, at the end of the reverse redrawing operation, at a distance from the cup base of: (a) 20 mm and (b) 45 mm.

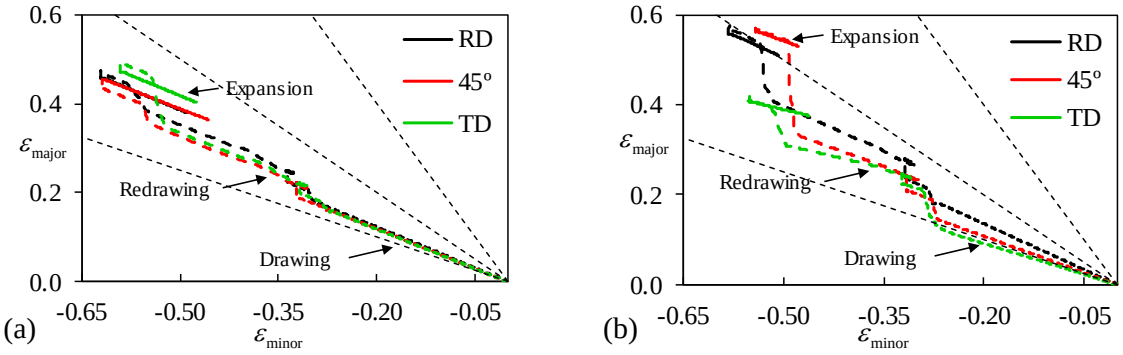

Figure 7. Numerical model: evolution of the principal in-plane strains at the leading edge of the cup at RD, 45º with RD and TD: (a) TH330 steel and (b) AA5352 alloy.

For the TH330 steel, the expansion punch attains the maximum displacement without the occurrence of any strain localization in the part. However, in the experimental tests, fracture occurred for a punch displacement of 30.2 mm, at an angle of 42º with RD, and banding was observed all around the free edge [5]. For the AA5352, as shown in Figure 5, the strain localization is predicted by both sets of anisotropy parameters, for similar displacements of the expansion punch and at identical orientations with RD. In the experimental tests, fracture occurred for a punch displacement of 16.4 mm, at an angle of 96º with RD [5].This means that both numerical results overestimate the punch displacement and the location.

The strain history (major and minor principal strains) of three points located in the upper surface of the cup (at RD, 45º and TD) is presented in Figure 7. Globally, the strain paths are similar for the three points. In the drawing operation, the strain path is situated between uniaxial compression and pure shear (middle and low dashed lines). Close to the end of the first stage, the points tend to plane strain. In the reverse redrawing operation, the strain path is, once again, between uniaxial compression and pure shear. Close to the end of this phase, the points tend to a plane strain path. Finally, the expansion operation corresponds to a strain path close to uniaxial tension. Globally, it is possible to observe that the points follow a more dissimilar trend for the AA5352, highlighting the fact that this material presents a more anisotropic behaviour than the TH330 steel. Also, for the AA5352 higher major strains are attained, particularly at the end of the reverse redrawing operation. This seems to be associated with the plane strain path, induced by the ironing stage. Note that only the results obtained with the set of anisotropy parameters labelled “AA5352” is plotted, which predicts strong thinning at the top of the cup at RD and close to 45º (see Figure 5). These strain paths will never cross the strain-based FLC and each material point will follow a different path, disabling a proper evaluation of formability based on that concept.

4. Conclusions

The comparison between the experimental and the numerical results shows that, globally, the cup height at the end of the reverse redrawing operations is well predicted. Nonetheless, the thickness distribution along the cup circumferential direction at two location from the bottom is underestimated, for both materials. For the AA5352 aluminium alloy this can be related with the occurrence of ironing of the wall in the numerical simulation, since the gap between the die and the punch of the redrawing stage does not allow to accommodate the thickening that occurs in the flange. Thus, the discrepancy can be associated with different process conditions. Moreover, it is known that formability also depends on this type of process parameters. However, for the TH330 steel the ironing never occurs. Thus, one can assume that the plastic flow is not accurately described by the normal to the yield surface. The analysis of the strain history for the points located in the upper surface of the cup (at RD, 45º and TD) highlights the fact that they are mainly submitted to stress states between uniaxial compression and pure shear. Unfortunately, this region of the yield surface is not covered by the set of experimental mechanical tests performed to characterize the mechanical behaviour of the material. Finally, regarding the prediction of strain localization, the simulations performed for the AA5352 aluminium alloy considering different sets of anisotropy parameters indicates that small changes can occur.

Acknowledgments

The authors would like to acknowledge the funding from of the Foundation for Science and Technology (FCT) under projects with reference PTDC/EME-EME/30592/2017 and PTDC/EME-EME/31243/2017 and by European Regional Development Fund (ERDF) through the Portugal 2020 program and the Centro 2020 Regional Operational Programme (CENTRO-01-0145-FEDER-031657) under project MATIS (CENTRO-01-0145-FEDER-000014) and UID/EMS/00285/2020.

References

[1] Keeler S P and Backofen W A 1963 Plastic instability and fracture in sheets stretched over rigid punches *Trans. Am. Soc. Met.* **56** 25–48
[2] Goodwin G M 1968 Application of strain analysis to sheet metal forming problems in the press shop *SAE Tech. Pap.* 380–7
[3] Stoughton T B and Zhu X 2004 Review of theoretical models of the strain-based FLDand their relevance to the stress-based FLD *Int. J. Plast.* **20** 1463–86
[4] Stoughton T B and Yoon J W 2012 Path independent forming limits in strain and stress spaces *Int. J. Solids Struct.* **49** 3616–25
[5] Watson M, Dick R, Huang Y H, Lockley A, Cardoso R and Santos A 2016 Benchmark 1 - Failure Prediction after Cup Drawing, Reverse Redrawing and Expansion *J. Phys. Conf. Ser.* **734** 022001
[6] Neto D M, Oliveira M C, Alves J L and Menezes L F 2015 Comparing faceted and smoothed tool surface descriptions in sheet metal forming simulation *Int. J. Mater. Form.* **8** 549–65
[7] Cazacu O and Barlat F 2001 Generalization of Drucker's yield criterion to orthotropy *Math. Mech. Solids* **6** 613–30
[8] Barros P D, Neto D M, Alves J L, Oliveira M C and Menezes L F 2015 DD3IMP, 3D Fully Implicit Finite Element Solver: Implementation of CB2001 Yield Criterion *Rom. J. Tech. Sci. – Appl. Mech.* **60** 105–36
[9] Volk W and Hora P 2011 New algorithm for a robust user-independent evaluation of beginning instability for the experimental FLC determination *Int. J. Mater. Form.* **4** 339–46
[10] Menezes L F and Teodosiu C 2000 Three-dimensional numerical simulation of the deep-drawing process using solid finite elements *J. Mater. Process. Technol.* **97** 100–6
[11] Oliveira M C, Alves J L and Menezes L F 2008 Algorithms and Strategies for Treatment of Large Deformation Frictional Contact in the Numerical Simulation of Deep Drawing Process *Arch. Comput. Methods Eng.* **15** 113–62
[12] Thuillier S, Manach P Y and Menezes L F 2010 Occurence of strain path changes in a two-stage deep drawing process *J. Mater. Process. Technol.* **210** 226–32